Advances in the Use of Geosynthetics for Stabilization of Unbound Aggregate Layers

Jorge G. Zornberg[1*], and *S* Subramanian[2]

[1] Professor, The University of Texas at Austin, 301 E. Dean Keeton St., Austin, TX 78712, USA
[2] PhD Student, The University of Texas at Austin, 301 E. Dean Keeton St., Austin, TX 78712, USA

Abstract. The governing mechanism associated with the stabilization of unbound aggregate layers in pavements is lateral restraint. Reproducing this mechanism in the laboratory maybe challenging because, while the original loading source is cyclic (traffic), lateral restraint develops through interlocking and interfacial friction between the geosynthetic and the aggregate to restrain the development of permanent lateral strains. Considering the relevance of lateral restraint in the quantification of the benefits of geosynthetics embedded within (or adjacent to) unbound aggregate layers, this study focuses on two experimental approaches to quantify this mechanism. The first experimental approach aims at defining a design parameter, identified as the Stiffness of the Soil-geosynthetic Composite (K_{SGC}), which is obtained from Soil-Geosynthetic interaction (SGI) tests and is practical for use in specifications and design. The second experimental approach that quantifies the lateral restraint mechanism involves one-third scale accelerated pavement tests (APTs), which were performed on pavement test sections stabilized with various geosynthetics, diverse in terms of geometry and materials. The rutting from these sections was compared to that in the non-stabilized (control) section to evaluate the Traffic Benefit Ratio (TBR) at failure rut depth for each geosynthetic. The TBR obtained showed a strong linear correlation to the K_{SGC} of the corresponding geosynthetic determined by SGI tests. Overall, the K_{SGC} parameter was found to represent a suitable indicator of the performance of pavements with unbound aggregate layers stabilized using geosynthetics.

1 Introduction

Geosynthetics have been successfully used within roadways systems to enhance the performance of paved and unpaved roads during service conditions under traffic and environmental loads. In fact, the number of applications of geosynthetics in roadways is large and growing. It includes ([1], [2]): the mitigation of reflective cracking in structural asphalt overlays, the reduction of layer intermixing, the reduction of moisture in structural layers, the stabilization of unbound aggregate layers, the stabilization of soft subgrades, and the mitigation of distress induced by the shrink/swell of subgrades.

* Corresponding author: zornberg@mail.utexas.edu

Early evaluation of the possible mechanisms involved in two of these roadway applications, the stabilization of unbound aggregate layers and the stabilization of soft subgrades, had been attributed to three common mechanisms: (1) lateral restraint, (2) increased bearing capacity, and (3) membrane tension support ([3]) As illustrated in Figure 1(a), the mechanism of lateral restraint involves the potential ability of the geosynthetic to minimize or eliminate the tendency of aggregates to move laterally. Such movement would in turn result in rutting on the pavement surface and, ultimately, serviceability failure. Geosynthetics with good interface shear resistance (or interlocking capabilities) and with adequate tensile stiffness were expected to provide resistance to such lateral movement of aggregates. Figure 1(b) shows an alternative geosynthetic mechanism in which the geosynthetic tensile forces intercept the original location of a critical shear surface associated with bearing capacity failure. In this case, the presence of the geosynthetic would force the critical shear surface to follow a different path, resulting in an increased resistance to bearing capacity failure of the system. Finally, Figure 1(c) illustrates a membrane-type support in which the vertical wheel load is partly resisted by the vertical component of the membrane tension that may develop within the geosynthetic. As long as relevant vertical deformations have occurred, and the geosynthetic has not reached its tensile strength, tension will develop in the geosynthetic to partly support the vertical traffic loads.

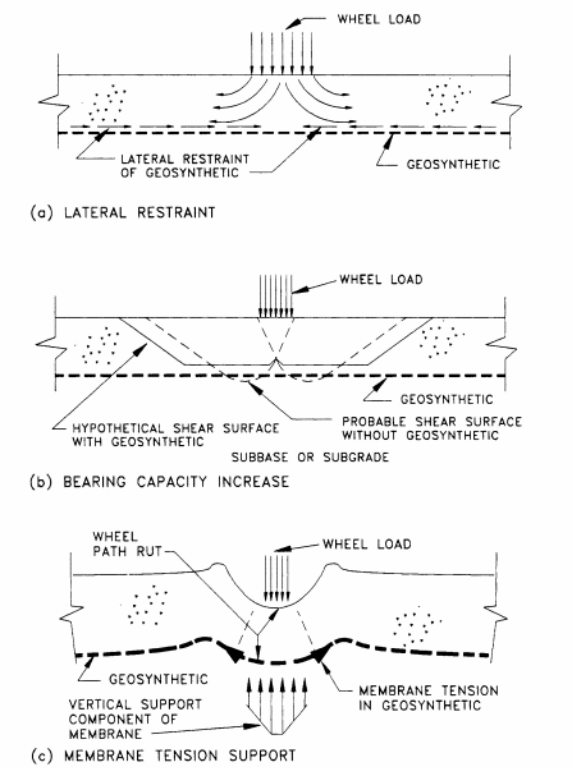

Fig. 1. Possible mechanisms provided by geosynthetics in roadways: (a) lateral restraint, (b) bearing capacity increase, and (c) membrane tension support ([3]).

Ultimately, the stabilization of unbound aggregates can be defined as the roadway application in which geosynthetics are used to increase (or to prevent a time-dependent decrease in) the stiffness of the unbound aggregate layer. Unlike applications involving stabilization of soft subgrades, the tensile strength of the geosynthetic is of no relevance and, instead, the confined stiffness of the aggregate-geosynthetic composite, under comparatively

small displacement, would be a key parameter. The geosynthetic tensile strength has been typically associated with applications that involve comparatively large displacements or deformations. Instead, stiffening, a geosynthetic function associated with its ability to develop tensile forces intended to control the deformation of the soil-geosynthetic composite, is key to characterize the lateral restraint mechanism. In fact, stiffening is the primary (and sole) function leading to decreased lateral displacements within (and increased confinement of) the soil-geosynthetic composite in the base layer. It should be noted that geosynthetic practitioners have also used the term 'stabilization' as the geosynthetic function identified herein as 'stiffening.' Instead, stabilization of unbound aggregates is considered herein as the roadway application and stiffening is adopted as the key geosynthetic function for this application.

While the geosynthetic could be placed within the base layer, its typical placement location to facilitate constructability is at the interface between the base being stabilized and the underlying subgrade. As previously discussed, the stabilization of unbound aggregate layers generally involves the mobilization of comparatively small geosynthetic strains while also requiring a high degree of interaction between the geosynthetic and the overlying base material. That is, the level of deformations is consistent with the small rutting depths expected in paved roads.

2 Background

The lateral displacement of aggregate particles, occurring under repeated traffic loading, represents a mechanism that degrades the mechanical properties of the aggregate base materials. Fig. 2(a) illustrates the lateral displacements that aggregates may develop within the base layer. The displacements result in decreased lateral stresses (i.e., decreased confinement) of the aggregate, which may significantly impact the modulus of the base material. In a multi-layer pavement system, the main characteristic of the base layer is its comparatively high modulus, which widens the distribution of vertical loads and ultimately decreases the maximum vertical stresses acting at the base-subgrade contact interface. Traffic-induced degradation of the original modulus in the aggregate results in increasing contact pressures at the base-subgrade interface and eventually high rutting depths in the roadway structure.

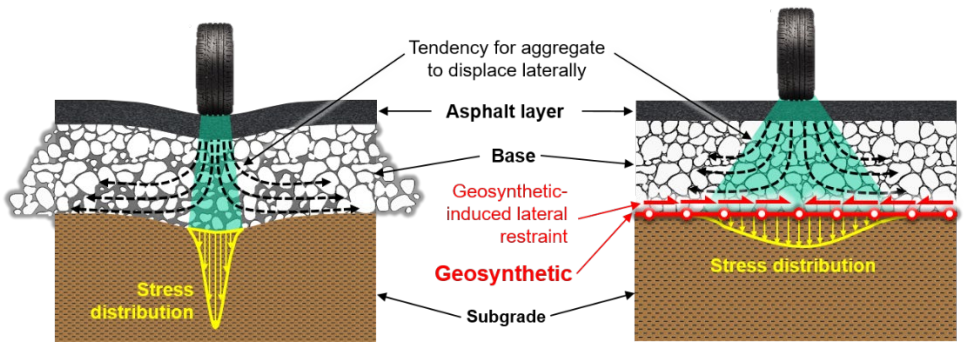

Fig. 2. Use of geosynthetics to stabilize unbound aggregate layers in roadways: (a) Non-stabilized road base, and (b) Stabilized road base ([1]).

Fig. 2(b) illustrates the restrain to lateral displacement provided by the geosynthetic inclusion. Interaction between the aggregate base and the geosynthetic results in transfer of shear stresses from the base material into tensile stresses in the geosynthetic. The tensile

stresses in the geosynthetic provide increased confinement in the base course material leading to an increase in the shear strength of the aggregate. Both frictional and interlocking characteristics of the soil-geosynthetic interface contribute to lateral restraint. Therefore, when geogrids are used to stabilize a road base, the geogrid aperture and base material particle sizes should be properly selected. On the other hand, when geotextiles are selected for base stabilization, proper interface frictional capabilities should be provided. As also illustrated in 2(b), the comparatively higher stiffness of the geosynthetic-stabilized base results in a wide distribution of traffic loads and in comparatively smaller vertical stresses acting at the base-subgrade contact.

A comparatively high interface shear transfer is needed to achieve stabilization of the base layer. In addition, the geosynthetic's own tensile stiffness contributes to limit the development of lateral strains. Consequently, a geosynthetic with comparatively high stiffness is required to achieve stabilization of the base. Zornberg et al. ([4]) identified a parameter, the stiffness of the soil-geosynthetic composite (K_{SGC}), which accounts for both the interface shear strength at the soil-geosynthetic interface and the geosynthetic stiffness.

Without the characterization of the K_{SGC}, geotechnical designers have relied on geosynthetics' mechanical properties in isolation to target a certain performance level. Ultimate tensile strength or tensile stiffness/modulus have frequently appeared on specifications, probably by assuming that the more strength or stiffness available for a particular product, the greater the potential for transfer of tensile stress from the surrounding aggregate ([5]). However, Giroud and Han ([6]) demonstrated no direct relationship between roadway performance and tensile strength at 5% strain after observing a set of full-scale tests undertaken on a wide range of different geogrid products. The reason being that the tensile strength of geosynthetic products in isolation does not represent the true behavior of the soil-geosynthetic composite in a roadway structure. Other studies have aimed at establishing correlations between geosynthetic index properties and their field performance. For geogrids, such index properties have included the geogrid junction strength, rib strength, wide-width tensile strength, tensile modulus, tensile strength at 2% and 5%, and flexural rigidity (e.g., [7], [8], [9], [10], [11]). However, once again, these index properties quantify the response of geosynthetics in isolation rather than under the confinement of soil.

An analytical model, referred to as the soil-geosynthetic composite (SGC) model, was developed at the University of Texas at Austin to provide a single parameter to characterize the confined stiffness of the soil-geosynthetic composite (K_{SGC}) under small displacements ([12], [13], [14], [4]). The SGC model involves a closed-form analytical solution that accounts for the geosynthetic confined stiffness, J_C, and the soil-geosynthetic interface shear, τ_y, both of which govern the performance of geosynthetic-stabilized roadways. The SGC model assumes a linear relationship between the geosynthetic unit tension T versus strain ε, characterized by J_C as seen in Figure 3(a). The SGC model also adopts a rigid–perfectly plastic relationship for the interface shear (τ) versus relative displacement (u), as shown in Figure 3(b), characterized by τ_y, the yield shear stress at the interface under confined conditions. The closed-form solution of the SGC model is characterized by a single parameter, the K_{SGC}, allowing for immediate implementation in project specifications. The K_{SGC} value is representative of a given soil-geosynthetic composite system, under a certain confining pressure, because it captures both the tensile characteristics of the confined geosynthetic and the shear behavior of the soil–geosynthetic interface ([4]). Solving the soil–geosynthetic force equilibrium differential equation defines the K_{SGC} as:

$$K_{SGC} = 4 \cdot \tau_y \cdot J_C \quad (1)$$

where J_C = the confined stiffness of the geogrid; and τ_y = the yield shear strength.

Therefore, the K_{SGC} of a geosynthetic is a measure that combines the in-isolation stiffness of the geosynthetic under confined conditions with the interaction of the geosynthetic and surrounding soil. A high K_{SGC} indicates that the geosynthetic under consideration is not only

stiff but also capable of significant stress transfer between the soil and geosynthetic. This implies that K_{SGC} is particularly well suited to determine how well a geosynthetic would perform stabilizing bases where the transfer of stresses from the soil to the geosynthetic is expected along with resistance to those transferred stresses (high stiffness).

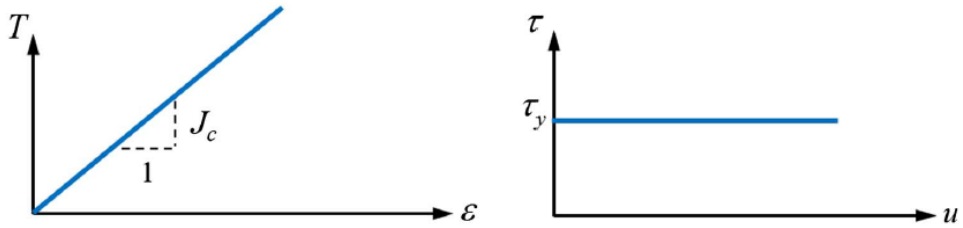

(a) (b)

Fig. 3. Constitutive relationships adopted in SGC model: (a) Linear unit tension-strain relationship for confined geosynthetic; (b) Rigid perfectly plastic soil–geosynthetic interface shear ([4]).

As will be discussed in Section 3 of this paper, the K_{SGC} can be determined experimentally in a pullout-like test setup provided that the frontal unit tension, internal displacements, and the frontal unit tension when the displacements are first mobilized within an embedded geosynthetic are measured (i.e., conditions at the onset of movement in each displacement measuring location). AASHTO-R50 ([15]) recommends performing full-scale tests with geosynthetics to predict their field performance. In the absence of full-scale field tests, correlations between geosynthetic properties and their field performance in stabilization can also be used ([5], [8]). However, these correlations may lack a mechanistic basis since they are based on properties that do not capture geosynthetic behavior under serviceable limits for surface pavements. This study proposes predicting stabilized pavement performance using the soil-geosynthetic composite stiffness, referred to herein as K_{SGC}, which captures the confined small-strain interaction of geosynthetics with soil.

3 Soil-geosynthetic Interaction Testing

The Soil-Geosynthetic Interaction (SGI) tests is a novel variation on a conventional pull-out resistance test that involves measurement of internal nodal displacements of the geosynthetic in addition to the external pull-out load and the corresponding frontal displacement of the geosynthetic ([16]). The small-scale soil-geosynthetic interaction equipment uses many of the basic components of a conventional pullout equipment, as described in the ASTM D6706-01(07) ([17]). However, there are a few critical differences. First, the soil volume used in the small-scale setup is only 5 % of the soil volume corresponding to the large-scale pullout device built with the minimum dimensions suggested in [17]. Second, the small-scale interaction test device pulls the geosynthetic specimen in the vertical direction. In this way, the soil-geosynthetic interaction test could be performed with load frames commonly used for wide-width tensile strength tests of geosynthetics, as specified by [18] and [19]. A general view of the soil-geosynthetic interaction setup is shown in Figure 4 [20].

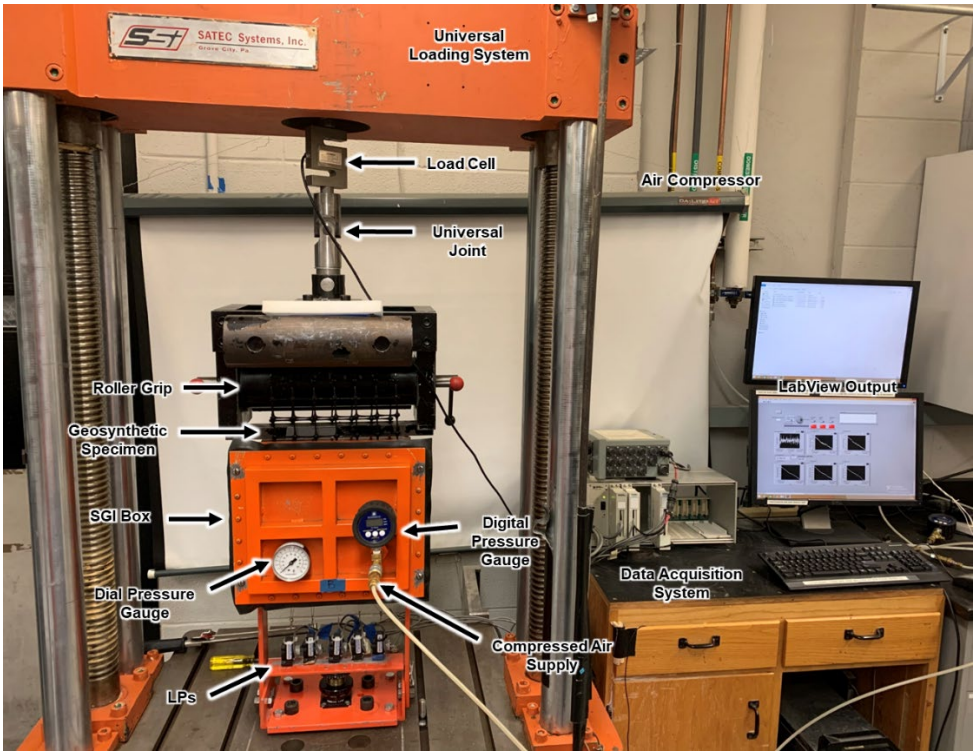

Fig. 4. Small-scale soil-geosynthetic interaction (SGI) test setup [20].

The soil-geosynthetic interaction box is made of steel with inner dimensions of 300 mm (11.8 in.) in width, 250 mm (9.8 in.) in length, and 150 mm (5.9 in.) in height, as shown in Figure 5. The front wall is manufactured with a horizontal rectangular opening with a width of 25 mm (1 in.) in the middle whereas the rear wall has a horizontal opening of 4 mm (0.16 in.) in the middle, as shown in Figure 5(a) and (b) respectively. The inner sides of the box are lined using Mylar® sheets attached to the SGI box using double-sided tape. This lining method aims to reduce the friction between the aggregate and the internal steel walls of the SGI box. The Mylar® sheets have a thickness of 0.007 in. (0.178 mm). Double-sided tape is used to prevent potential sliding of the Mylar® sheet during aggregate placement and as the test progresses.

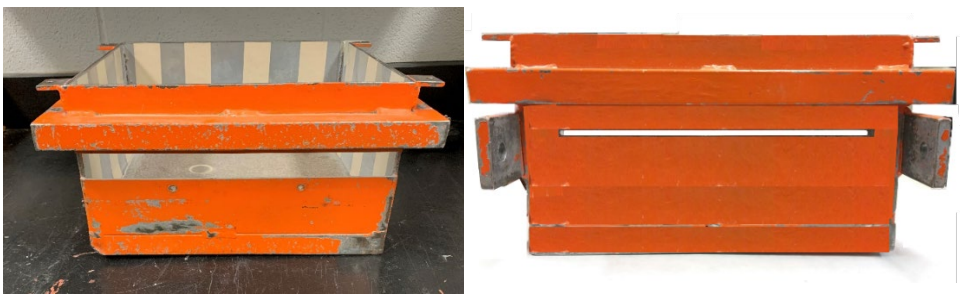

(a) (b)

Fig. 5. Soil-geosynthetic interaction box: (a) Front view, (b) Back view [20].

The confining pressure is applied using compressed air in a flexible bladder attached to the lid of the SGI box, as shown in Figure 6. The bladder can be inflated up to 6 psi. A piece of non-woven geotextile is placed on top of the soil backfill to protect the air bladder from puncture. A digital and a dial pressure gauge are used to control the confining pressure. The digital pressure gauge manufactured by SSI Technologies Inc has a range of 0-30 psi and accuracy ± 0.25%.

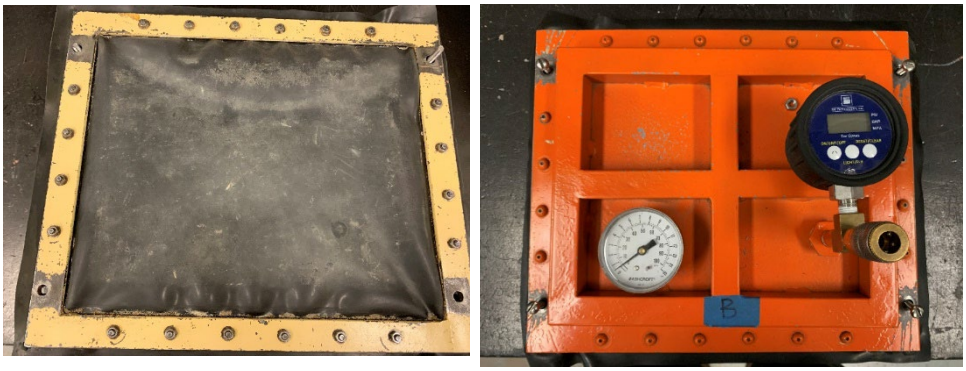

(a) (b)

Fig. 6. Views of the SGI box: (a) Bottom view with the inflated air bladder; (b) Top view with digital air pressure gauge to be connected to air pressure supply and dial pressure gauge [20].

The load frame used for the soil-geosynthetic interaction test, manufactured by Satec Systems Inc. (SN 60CG-1009), consists of a roller grip that pulls the geosynthetic specimen in the vertical direction. A supporting frame is fixed to the base of the loading frame below the geosynthetic test box. The displacement measuring sensors are securely mounted onto the supporting frame, as seen in Figure 7. A 5000 lbf. S-shape load cell manufactured by Omega Engineering (SN 1457992), referred to as SGI load cell, is used to measure the pullout load. The load cell is attached to the roller grip using a universal joint.

Five UniMeasure LX-PA linear potentiometers (LPs) are used to measure displacements at five distinct locations across the geosynthetic specimen, referred to as telltale points. The LPs have a measuring range of 2.8 in. (7.11 cm). A data acquisition system (DAS) is used to convert an analog voltage output into a digital signal that can be recorded as a numerical value to be processed by a computer. Zinc-galvanized steel wires, 1.04 mm (0.041 inch) in diameter, connect tell-tale points (i.e., displacements measuring locations across the geosynthetic specimen) in the confined portion of the geosynthetic specimen to the LPs. The steel wires have small hooks at both ends; one end is attached to the geosynthetic, and the other joins the wire to the corresponding LP.

The width of the confined portion of the geosynthetic specimen is 280 mm ± 5 mm (11.0 in. ± 0.2 in.). The adjustment of ± 5 mm (0.2 in) is to accommodate different aperture sizes of geosynthetic products. The zinc-galvanized steel wires described above are attached at five different junctions along the embedded length of the geogrid in a staircase fashion, as seen in Figure 8. These wires are then attached to the displacement sensors to obtain the displacement along the geosynthetic specimen mobilized during the test.

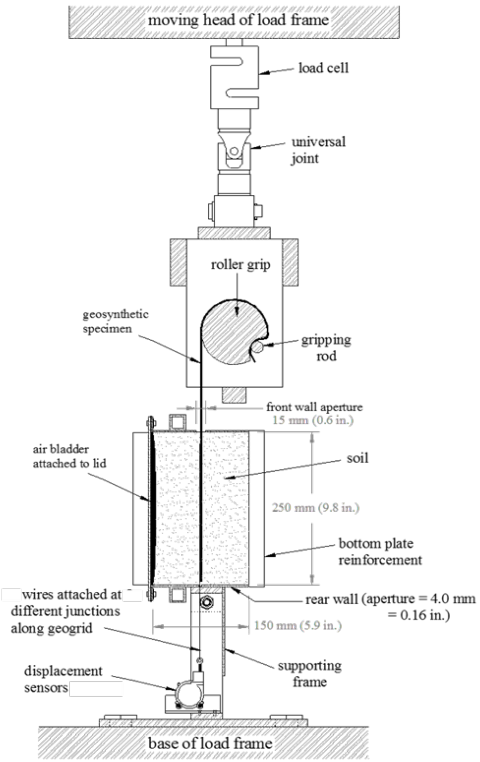

Fig. 7. Side view of various components of the loading system ([21]).

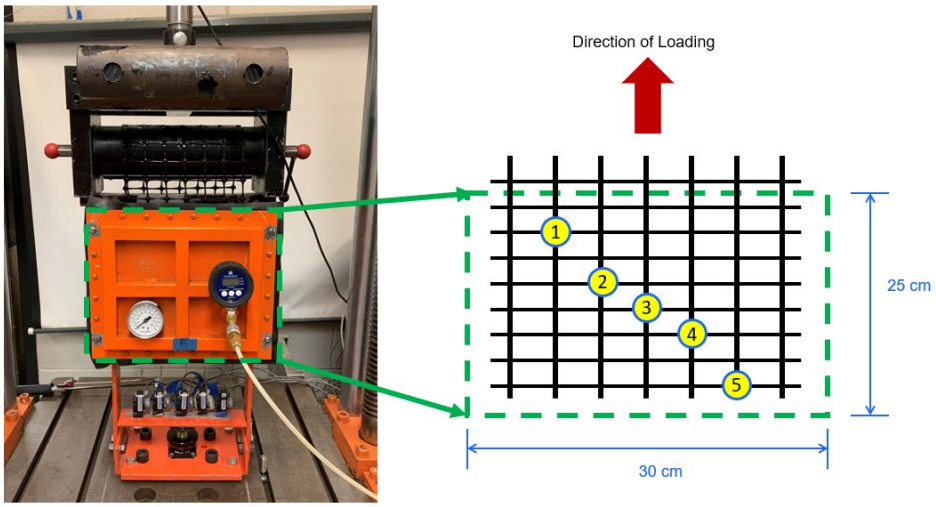

(a) (b)

Fig. 8. SGI testing: (a) Plan view of the small pullout test setup at UT Austin; (b) Location of points of monitored displacements along the geosynthetic specimen [20].

4 Results from the Soil-geosynthetic Interaction (SGI) Tests

A total of four types of geosynthetics (GG1 to GG4), illustrated in Figure 9, were adopted in this investigation. These products differ in their material and geometric properties as summarized in Table 1.

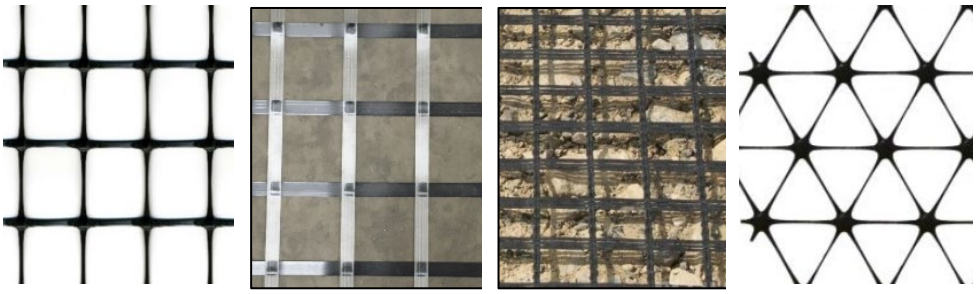

(a) (b) (c) (d)

Fig. 9. Geosynthetics used in the experimental programs (SGI and MMLS testing): (a) GG1, (b) GG2, (c) GG3, (d) GG4.

The SGI tests performed for this study involved sandwiching each geosynthetic (GG1 to GG4) within a clean gravel base material, conforming to the AASHTO #8 gradation. The tests were performed at a confining pressure of 21 kPa. The geosynthetics were pulled out from the soil-geosynthetic matrix while measuring their internal nodal displacements under the applied frontal unit tension.

Table 1. Index properties specified by the geosynthetic manufacturers.

Property	GG1	GG2	GG3	GG4
Polymer Type	PP	PP	PP	PP
Manufacturing Process	Punched Drawn	Welded Strips	Woven Yarns	Punched Drawn
Aperture Shape	Rect.	Rect.	Rect.	Triangle
Aperture Dimensions (mm)	33 x 25	41 x 41	15 x 15	33
Rib Width (mm)	3.2	9.0	-	1.0
Minimum Rib Thickness (mm)	0.76	0.6	-	2.0
Tensile Strength @ 1% Strain (kN/m)	-	5.2	-	-
Tensile Strength @ 2% Strain (kN/m)	6.6	8.2	7	-
Tensile Strength @ 5% Strain (kN/m)	13.4	15.1	14	-
Ultimate Tensile Strength (kN/m)	19.0	24.2	23.3	-
Junction Efficiency (%)	93	-	-	93

The frontal unit tension, T, and displacements, u, are directly measured in the geosynthetic specimen at the location of the telltales, as shown in Figure 10 [20]. Figure 10 also illustrates the progressive mobilization of the interface shear along the geosynthetic. The displacements corresponding to LP1 (connected to the geosynthetic node closest to the pulling front) start mobilizing at a relatively low unit tension, whereas LP5 requires a much larger unit tension. As the unit tension increases, LPs 2, 3, 4, and 5 are successively triggered.

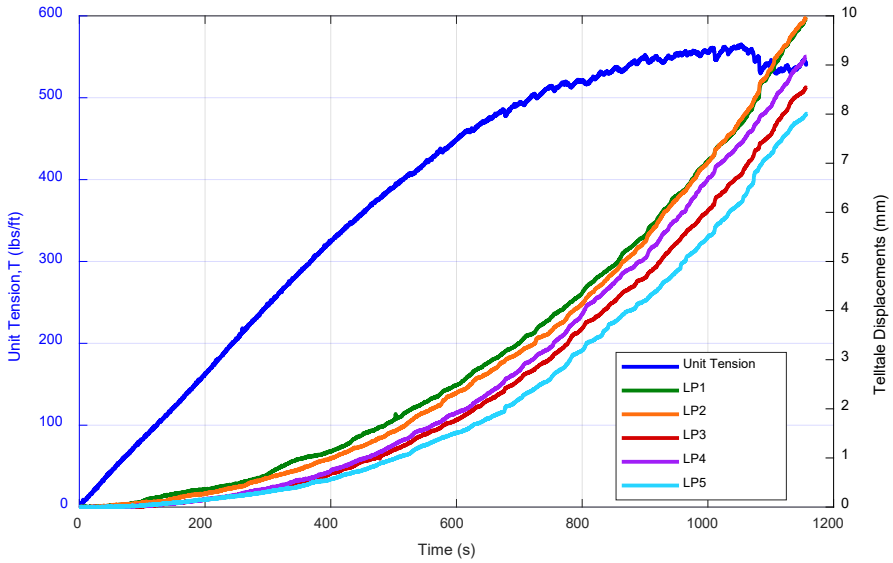

Fig. 10. Frontal unit tension and geosynthetic displacement versus time in a typical SGI test [20].

Figure 11 illustrates a typical plot of the frontal unit tension versus displacement along the geosynthetic. The frontal unit tension reaches a state of maximum constant tensile load, which is defined as the pullout failure [20]. The tests in this program were carried out up to pullout failure.

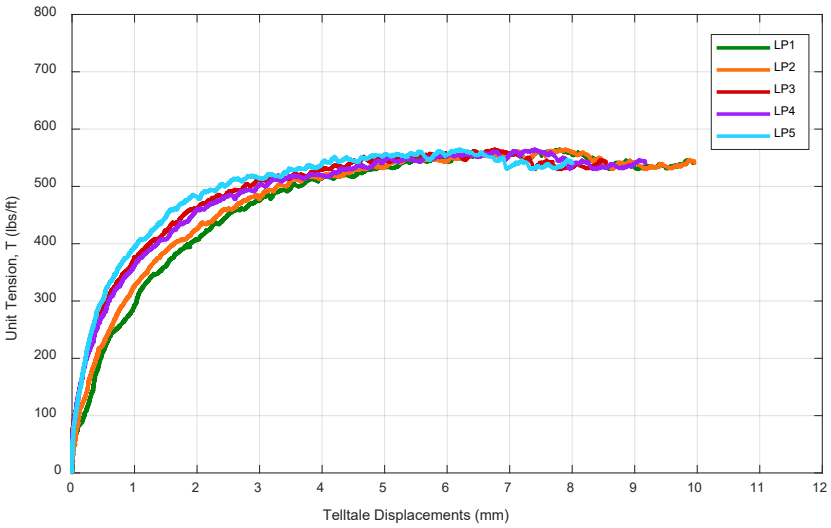

Fig. 11. Frontal unit tension versus measured displacements at the location of each telltale [20].

According to the SGC model, the K_{SGC} is defined as the slope of T^2 versus u data after the onset of the tell-tale movements at the location of the geosynthetic node. Thus, the unit tension when the displacements are first mobilized at a given tell-tale location must be determined. Specifically, the unit tension T_i at the location of tell-tale i can be obtained using measurements of the frontal unit tension collected when displacements at tell-tale i are first

triggered, $T_{o,i}$ ([4]). For each telltale location, the unit tension values are shifted by the unit tension value measured at the time the telltale location exceeds the triggering point ($T_i = T - T_{o,i}$). The SGI test procedure suggests using 0.1 mm as the triggering point. This value allows not to misinterpret the noise recorded by the linear potentiometers as actual tell-tale movements at the onset of the displacement. Furthermore, the displacements that are accounted for in the estimation of K_{SGC} should correspond to those mobilized by soil-geosynthetic interaction; that means displacements that are realized by relatively small unit tensions (e.g., following initial adjustment of the geosynthetic after applying a seating load) should not be used. Figure 12 shows the relationship between the unit tension squared and displacements at the location of telltales 2, 3, and 4 [20]. Since the K_{SGC} is a small-strain stiffness, only geosynthetic displacements ranging from 0.1 mm to 1.0 mm are used for the K_{SGC} calculation. The K_{SGC} is obtained using linear regression on the T^2 versus u data for each telltale location.

A total of five SGI repeat tests were conducted in this study for each geosynthetic and three nodal displacements were measured per test. Thus, the K_{SGC} was calculated as the slope of the square of the unit tension (in (kN)/m) at each node versus the nodal displacement (in mm) of the corresponding node. The K_{SGC} of each geosynthetic was taken as the mean of the 15 K_{SGC} values obtained as previously discussed.

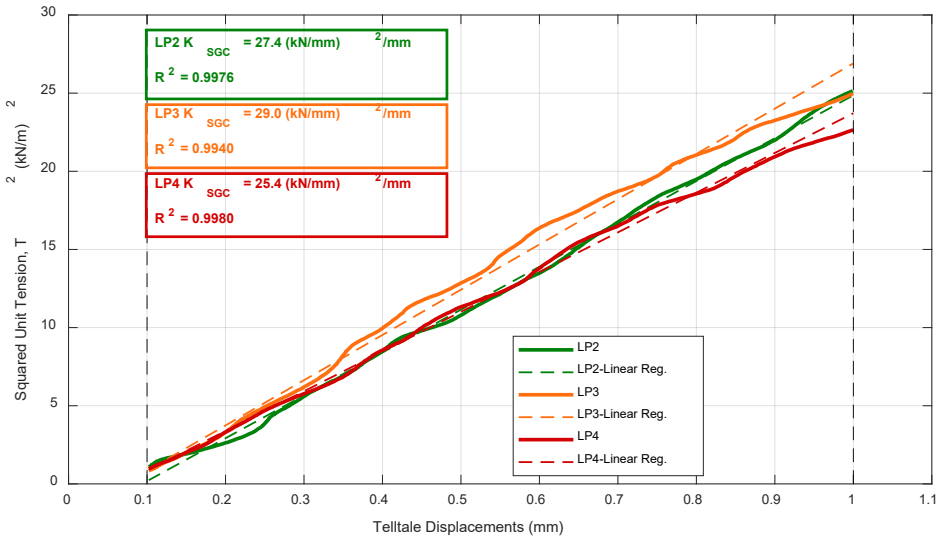

Fig. 12. K_{SGC} Results for LPs 2, 3, and 4 (center area of confined geosynthetic specimen) [20].

The K_{SGC} of the four geogrids (GG1, GG2, GG3, and GG4) used in this study were found to be between 9 (kN/m)^2/mm and 20 (kN/m)^2/mm. Specifically, the geogrid GG2, noted to have the highest tensile strength characteristics from Table 1, performed the worst with a K_{SGC} of 9.6 (kN/m)^2/mm. Geogrid GG1, with the lowest tensile strength, had a K_{SGC} of 13.7 (kN/m)^2/mm. Geogrid GG3, with the smallest aperture opening and high tensile strength performed the second best with a K_{SGC} of 15.6 (kN/m)^2/mm. Geogrid GG4, with the triangular opening, lower rib width and higher rib thickness, performed the best with a K_{SGC} of 18.8 (kN/m)^2/mm. Thus, the K_{SGC} of the four geogrids were not correlated with the strength, stiffness or geometric properties of the geogrids.

5 Accelerated Pavement Testing

To assess the performance of pavement sections with a stabilized base course, reduced-scale pavement sections were constructed in the laboratory under controlled environmental conditions. These sections had identical pavement configurations but used the four different types of geosynthetics discussed in Section 4 of this paper and illustrated in Figure 9 (GG1 to GG4). Another section was constructed without a stabilizing geosynthetic to serve as the control. All five pavement sections consisted of a 15-cm clean, uniform sand subgrade placed at 67% relative density; 12.5-cm gravel base, which conformed to AASHTO#8 gradation, placed at 85% relative density; and 2.5-cm Hot Mix Asphalt (HMA) ride surface from a thin overlay mix – type A (TxDOT SS3239 ([21])). The entire structure was built above grade in two modular 15-cm-tall frames. The pavement structure was 180 cm (72") in length and width, with a total depth of 30 cm, as shown in Figure 13. The geosynthetic in the stabilized sections was placed 7.5 cm below the HMA surface within the base.

Accelerated Pavement Tests (APTs) were conducted on all five sections using the model mobile load simulator (see Fig. 14) by applying repeated, unidirectional, rolling-wheel loads of 2.1 kN at 620 kPa tire pressure. The pavement structure was subjected to 7,200 load repetitions per hour. Additional details on the loading equipment and its capabilities can be found in previous studies such as [22].

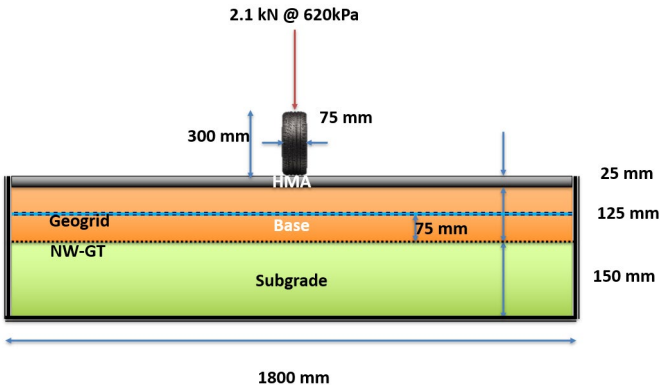

Fig. 13. Cross-section of pavement model.

Fig. 14. Model Mobile Load Simulator (MMLS) trafficking a pavement test section.

A Laser Distance Meter (LDM) attached to the carriage on an actuator was used to profile the surface deformations as presented in Figure 15. By controlling the LDM sampling rate and actuator velocity, the vertical distance from the actuator to the pavement surface was captured for every 5 mm of horizontal actuator displacement. This allowed for the generation of transverse surface profiles with 360 sample points. The pavement was painted white at the profiling locations to improve the reflectivity of the laser. The post-trafficking surface profiles were compared to the initial surface profile to determine rutting at any given number of passes.

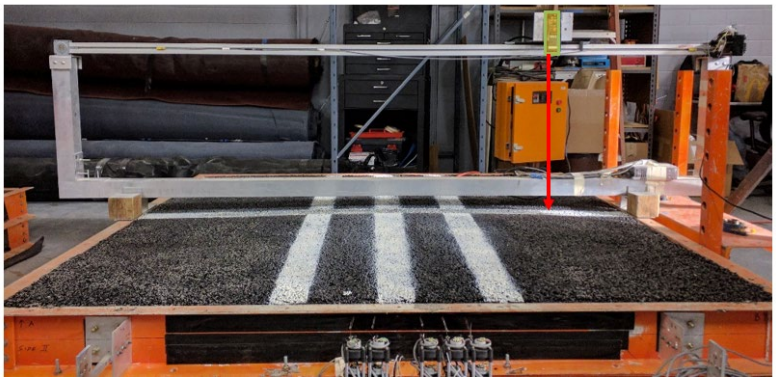

Fig. 15. Profilometer mounted on pavement test section (laser distance meter is highlighted in green).

6 Results from the Accelerated Pavement Tests (APTs)

The performance of the various pavement sections was measured in terms of rutting. Rutting was measured from the post-trafficking surface deformation profiles, after correcting for pre-trafficking surface. As indicated in Figure 16, rutting is measured as the maximum depth from the top of the heave next to the wheel path to the path of the trough under the wheel path . Rut measurements were taken periodically after a pre-determined number of wheel passes. Figure 17 shows the rut measurements taken until failure of all five pavement sections with and without geosynthetic stabilization.

The improvement in pavement performance due to the stabilization of the base course can be quantified using the Traffic Benefit Ratios (TBRs) obtained by comparing the rutting in the geosynthetic-stabilized sections (GG1 to GG4) to that in the control section. This comparison is possible because the only difference between each geosynthetic-stabilized sections and the control section was the presence of a geosynthetic. Consequently, the TBRs for each stabilized section are a direct measure of the improvement attributable to the corresponding geosynthetic.

For the purposes of this study, a TBR due to geosynthetic stabilization is defined as the ratio of the number of load repetitions up to failure in the stabilized section to that in the control section, given the identical pavement structure aside from the geosynthetic. From Figure 17, the number of wheel passes to various levels of rut are indicated and their TBR is determined as follows:

$$TBR_{RD} = \frac{N_{GSS}}{N_{Control}} \tag{2}$$

where TBR_{RD} = the Traffic Benefit Ratio at failure, defined as rut = RD; N_{GSS} = the number of wheel passes to failure rut, RD, in the geosynthetic-stabilized section; and $N_{Control}$ = the number of wheel passes to failure rut, RD, in the control section.

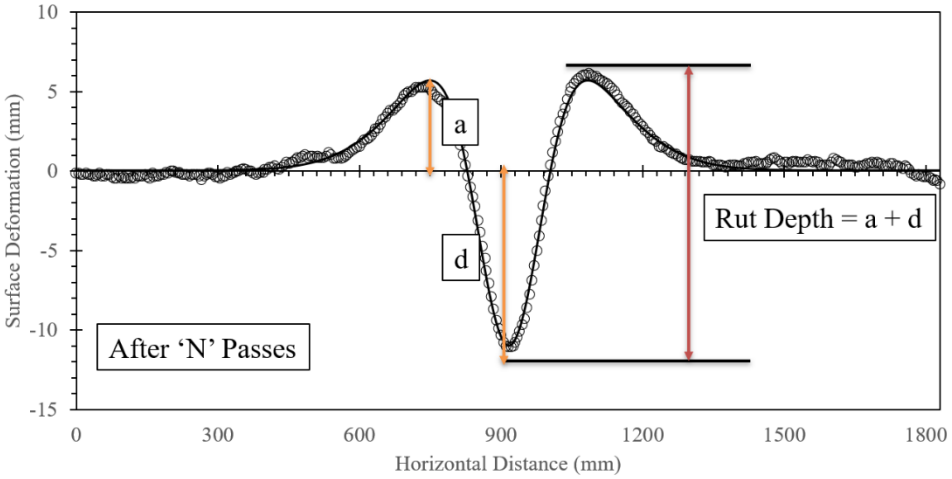

Fig. 16. Typical rutting profile with 360 sample points from laser profilometer .

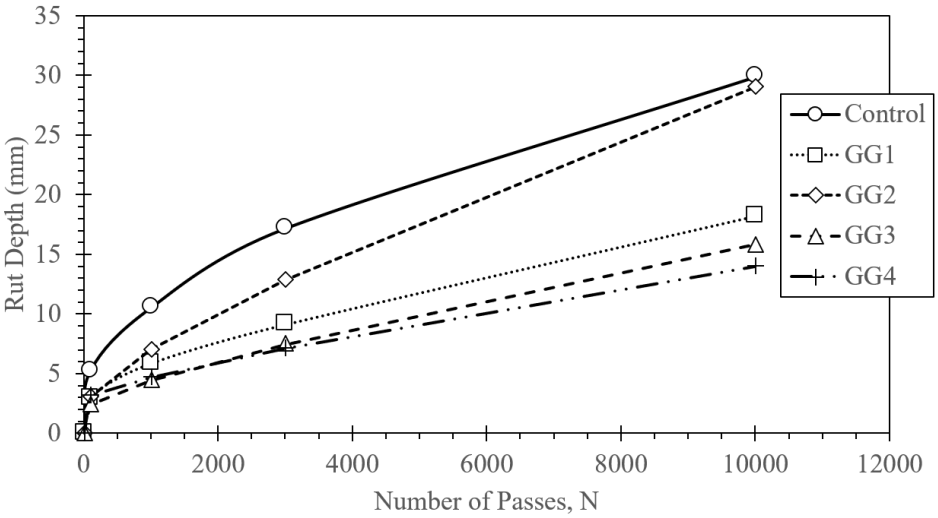

Fig. 17. Progression of rutting with trafficking on all test sections.

Thus, the TBR for the various stabilized sections can be expressed as a function of the rut depth, as shown in Figure 18. The TBR starts at 1.0 for very small rutting values, then increases rapidly to a maximum rut depth in the range of 2.5 mm to 5 mm , and ultimately decreases and asymptotes to a constant rut depth of around 10 mm to 15 mm . This is likely due to the high relative density (85%) of the base layer within which the geosynthetic is placed. As the pavement surface is trafficked, the dense base layer in the control section begins dilating . But in the geosynthetic-stabilized sections, the dilatancy is reduced ([23], [11]), resulting in increased TBR. As the deformations increase, the base material reaches its critical state, so benefits from the geosynthetic reduce and asymptote to a constant TBR value.

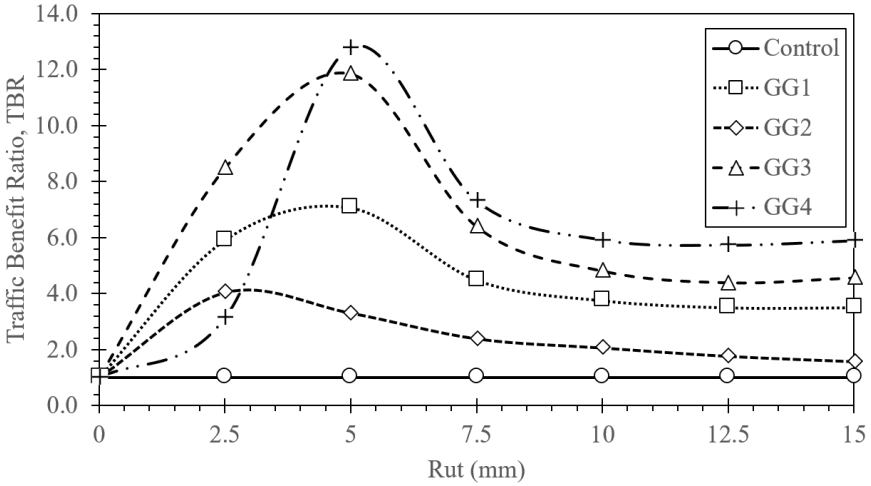

Fig. 18. TBR as a function of rut for geogrid-stabilized sections.

7 Correlation between SGI and APT Results

Figure 19 compares the TBR obtained after reaching the aggregate critical state for each geosynthetic-stabilized section with the K_{SGC} obtained from SGI tests between the same geosynthetic and base material. Each circle represents the (TBR, K_{SGC}) pair for a particular geosynthetic. The dashed line is the linear regression line through the datapoints. As can be seen in the figure, the TBR of any stabilized section is linearly correlated with the K_{SGC} of the base course-geosynthetic composite used in the stabilized sections. The high degree of linear correlation ($R^2 = 0.9994$) between TBR and K_{SGC} values confirms that K_{SGC} is a direct measure of the improvement to pavement rutting performance due to the geosynthetic inclusion and is thus a strong justification for the use of K_{SGC} as a critical parameter in the selection of geosynthetics for base stabilization.

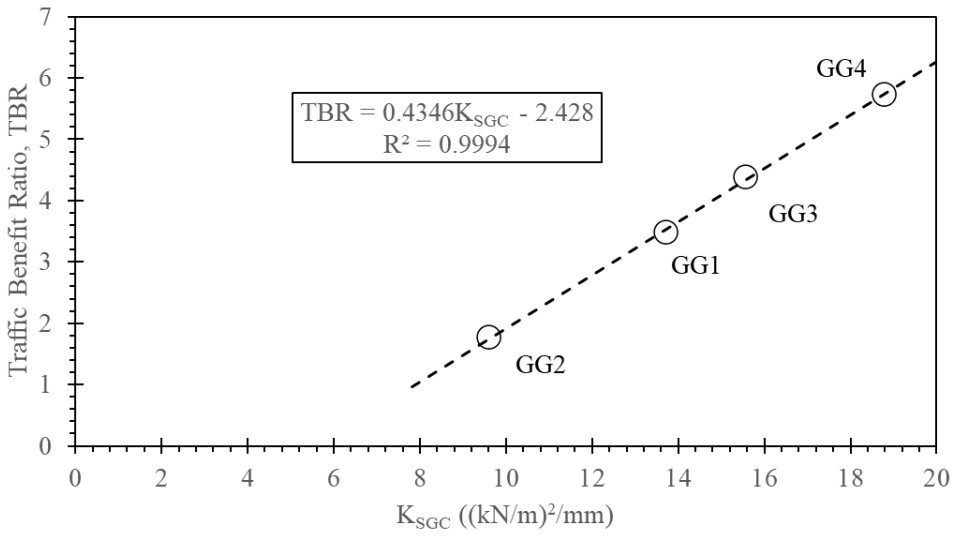

Fig. 19. TBR vs. K_{SGC}..

8 Conclusions

Reduced-scale Accelerated Pavement Tests (APTs) and Soil-Geosynthetic Interaction (SGI) tests were conducted using AASHTO#8 base material and four different types of geosynthetics. From SGI tests, the K_{SGC} of the base material-geosynthetic composite for all four geosynthetics was determined to range from 9 $(kN/m)^2/mm$ to 20 $(kN/m)^2/mm$. The Traffic Benefit Ratio (TBR) was used to quantify the improvement in traffic performance due to the geosynthetic inclusion through comparison with a non-stabilized control section. The TBR values were found to be a function of the failure rut depth. The TBR was found to increase with increasing rut depth up to a maximum TBR value and then decrease to an asymptotic value. This interesting behavior observed for the stabilized sections can be attributed to the dilation of the base material and varying levels of reduced dilatancy facilitated by the stabilizing geosynthetic.

The asymptotic TBR of the stabilized sections was also found to differ by the type of geosynthetic used, as it exhibited strong linear correlation to the base material-geosynthetic composite stiffness determined from SGI tests. Consequently, K_{SGC} can therefore be used to predict the performance of geosynthetic-stabilized base layers in flexible pavements and to aid in the selection of geosynthetics for roadway applications involving the stabilization of unbound aggregates.

References

1. Zornberg, J.G. (2017). “Geosynthetics in Roadway Infrastructure.” *Procedia Engineering*, Elsevier, Transportation Geotechnics and Geoecology, May, Vol. 189, pp. 298-306.
2. Zornberg, J.G. and Tutumluer, E. (2021). “Summary of Applications Involving Geosynthetics in Transportation Infrastructure.” *Training Material*, Short course on Geosynthetics in Roadways, Railways, and Airfields.
3. Haliburton, T.A., Lawmaster, I.D. and McGuffey, V.C., Use of Engineering Fabrics in Transportation Related Applications, FHWA DTFH61-80-C-Q0094, 1981.
4. Zornberg, J.G., Roodi, G.H., & Gupta, R. 2017. “Stiffness of Soil-geosynthetic Composite under Small Displacements: I. Model Development.” Journal of Geotechnical and Geoenvironmental Engineering, ASCE, Vol. 143, No. 10, October.
5. Archer S. & Wayne M. H. 2012. "Relevancy of Material Properties in Predicting the Performance of Geogrid-Stabilized Roadway." Proc. of the conference GeoFrontiers, Advances in Geotechnical Engineering, ASCE, Oakland, California, pp.1320-1329
6. Giroud, J.P., and Han, J. (2016). “Mechanisms Governing the Performance of Unpaved Roads incorporating Geosynthetics: Part 1.” *Geosynthetics,* Industrial Fabrics Association International, June.
7. Perkins, S.W., Christopher, B. R., Cuelho, E.L., Eiksund, G.R., Hoff, I., Schwartz, C.W., Svano, G., and Want, A. (2004). “Development of Design Methods for Geosynthetic Reinforced Flexile Pavements.” *U.S. Department of Transportation, Federal Highway Administration*, Report No. FHWA-DTFH61-01-X-00068, Final report., Washington, D.C., USA, 263p.
8. Christopher, B.R., Cuelho, E.V., and Perkins, S.W. (2008). “Development of Geogrid Junction Strength Requirement for Reinforced Roadway Base Design.” *In Proceeding of GeoAmericas 2008 Conference*, Cancun, Mexico, 2008.

9. Cuelho, E., and Perkins, S. (2005). "Resilient Interface Shear Modulus from Short Strip Cyclic Pullout Tests." *Geofrontiers: Slopes and retaining structures under seismic and static conditions*, ASCE GSP-140, Austin, TX.
10. Mahmood, T., Hatami, K., Ghabchi, R., and Zaman, M.M. (2012). "Pullout Performance of Geogrids with Different Junction Strength." *Proceeding of the Geo-Congress 2012: State of the Art and Practice in Geotechnical Engineering*, Oakland, CA, USA, pp. 1360-1370.
11. Chen, X., Jia, Y. and Zhang, J., 2018. Stress-strain response and dilation of geogrid-reinforced coarse-grained soils in large-scale direct shear tests. Geotechnical Testing Journal, 41(3), pp.601-610.
12. Gupta, R., (2009). *A Study of Geosynthetic-Reinforced Flexible Pavement System*. PhD Dissertation, The University of Texas, Austin, Texas, USA, 318p.
13. Roodi, G. H. (2016). *Analytical, Experimental, and Field Evaluations of Soil-geosynthetic Interaction under Small Displacements.* Ph.D. dissertation, The University of Texas, Austin, Texas, August 2016, 623 p.
14. Roodi, G. H., and Zornberg, J. G. (2017). *"Stiffness of Soil-Geosynthetic Composite under Small Displacements: II. Experimental Evaluation"* Journal of Geotechnical and Geoenvironmental Engineering, ASCE, Vol. 143, No. 10, 10.1061/(ASCE) GT.1943-5606.0001769, 04017076.
15. AASHTO R50. 2009. Standard Practice for Geosynthetic Reinforcement of the Aggregate Base Course of Flexible Pavement Structures. American Association of State Highway and Transportation Officials, Washington, D.C.
16. Roodi, G.H., & Zornberg, J.G. 2017. "Stiffness of Soil-geosynthetic Composite under Small Displacements. II: Experimental Evaluation." Journal of Geotechnical and Geoenvironmental Engineering, ASCE, Vol. 143, No. 10, October.
17. ASTM D6706-01(07) (2007). "Standard Test Method for Measuring Geosynthetic Pullout Resistance in Soil." American Society for Testing and Materials, West Conshohocken, PA, USA, 8p.
18. ASTM D4595-11 (2011). "Standard Test Method for Tensile Properties of Geotextiles by the Wide-Width Strip Method." *American Society for Testing and Materials*, West Conshohocken, PA, USA, 13p.
19. ASTM D6637/D6637M-15 (2015). "Standard Test Method for Determining Tensile Properties of Geogrids by the Single or Multi-Rib Tensile Method." *American Society for Testing and Materials*, West Conshohocken, PA, USA, 6p.
20. Peve, L. (2020). M.S. Thesis: "Sources of Variability in Small-scale Soil-geosynthetic Interaction Testing." Department of Civil, Architectural, and Environmental Engineering. The University of Texas at Austin.
21. TxDOT SS3239. 2004. Special Specification for Thin Overlay Mix (TOM). TxDOT
22. Epps Martin, A., Walubita, L.F., Hugo, F. and Bangera, N.U., 2003. Pavement response and rutting for full-scale and scaled APT. Journal of Transportation Engineering, 129(4), pp.451-461.
23. Sweta, K. and Hussaini, S.K.K., 2019. Behavior evaluation of geogrid-reinforced ballast-subballast interface under shear condition. Geotextiles and Geomembranes, 47(1), pp.23-31.